

# INTERPRETING AND EDITING VISION-LANGUAGE REPRESENTATIONS TO MITIGATE HALLUCINATIONS

Nick Jiang\*, Anish Kachinthaya\*, Suzie Petyrk†, Yossi Gandelsman†

University of California, Berkeley

{nickj, anishk, spetryk, yossi\_gandelsman}@berkeley.edu

## ABSTRACT

We investigate the internal representations of vision-language models (VLMs) to address hallucinations, a persistent challenge despite advances in model size and training. We project VLMs’ internal image representations to their language vocabulary and observe more confident output probabilities on real objects than hallucinated objects. We additionally use these output probabilities to spatially localize real objects. Building on this approach, we introduce a knowledge erasure algorithm that removes hallucinations by linearly orthogonalizing image features with respect to hallucinated object features. We show that targeted edits to a model’s latent representations can reduce hallucinations by up to 25.7% on the COCO2014 dataset while preserving performance. Our findings demonstrate how a deeper understanding of VLMs’ latent representations can enhance reliability and enable novel capabilities, such as zero-shot segmentation.<sup>1</sup>

## 1 INTRODUCTION

Vision-Language Models (VLMs) have recently emerged as powerful tools for understanding images via text (Dai et al., 2023; Liu et al., 2024a). They have demonstrated remarkable capabilities across multimodal tasks such as image captioning (Li et al., 2023a), visual question answering (Ye et al., 2023), and complex multimodal reasoning (Bai et al., 2023). Despite their capabilities, VLMs tend to hallucinate content that does not appear in the images (Ji et al., 2023), which poses serious concerns for the reliability of these models in real-world applications (Hu et al., 2023; Luo et al., 2024).

Widespread belief has been that scaling to larger models and more training data will naturally mitigate hallucinations. However, recent studies have shown that hallucinations persist even in larger and more advanced models (Rohrbach et al., 2019; Li et al., 2023b), suggesting that this issue cannot be solved by scale alone. Current methods reduce hallucinations by applying external interventions (e.g. object detectors; Yin et al. (2023)) or additional model fine-tuning (e.g. on hallucination examples; Zhou et al. (2024); Zhang et al. (2024a)). Nevertheless, these methods often struggle to distinguish between subtle hallucinations and existing details, requiring new models or updated model parameters.

In this paper, we aim to introduce fine-grained edits directly to the image latent representations of VLMs to reduce hallucinations without hindering their performance, an approach that has had some success in large language models (Zhang et al., 2024b; von Rutte et al., 2024). To edit the latent representations of VLMs, we first explain their role via text. We employ the logit lens technique (nostalgebraist, 2020) to directly interpret the spatial VLM *image* representations with VLM *text vocabulary*. Surprisingly, the characteristics of these image representations are different for real objects that appear in the image and objects that are hallucinated. Moreover, the logit lens enables spatially localizing objects within the input image.

Relying on the ability to detect hallucinated objects, we edit them out by intervening in their internal representations. We introduce a knowledge erasure algorithm, PROJECTAWAY, to target and remove objects by linearly orthogonalizing image features with respect to the text features of target objects. We find that PROJECTAWAY can erase both real and hallucinated objects with high rates of removal.

\*Equal contribution as first authors.

†Equal contribution as last authors.

<sup>1</sup>Code: <https://github.com/nickjiang2378/vl-interp>

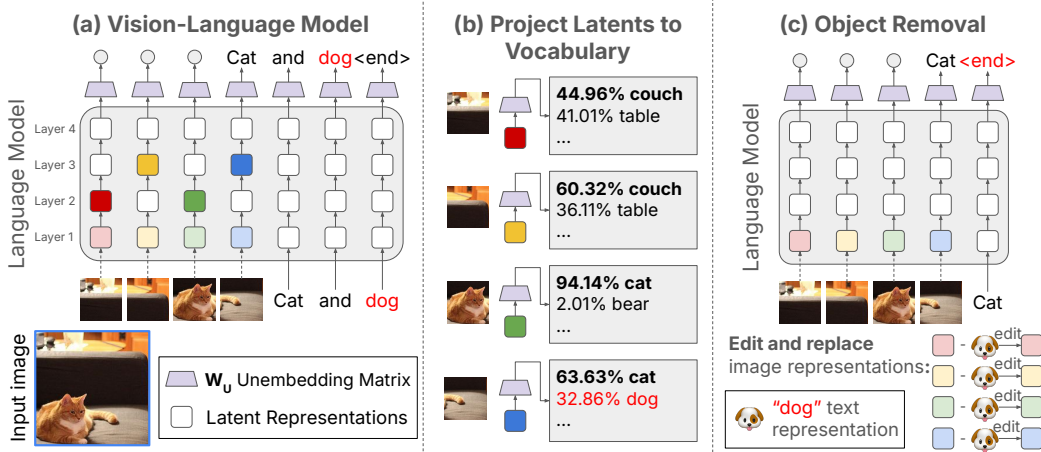


Figure 1: **Interpreting VLM internal image representations.** (a) Given a VLM, (b) we unembed the latent representations from image embeddings to the vocabulary and classify hallucinations. We remove hallucinations by (c) linearly editing them out of the latent representations.

We use our interpretation and editing approach for three tasks. First, we utilize the logit lens on image features to detect hallucinations in the image. We find that it improves mAP by 22.45% and 47.17% in two VLMs. Then, we combine our editing and detection method to erase hallucinations from the VLM’s internal representations, reducing hallucinations up to 25.7% on standard benchmarks, while preserving accuracy in image captioning. Finally, we use the logit lens to localize objects in the image features. We find that our spatial mapping provides comparable performance to state-of-the-art zero-shot segmentation methods. Our results indicate that understanding the internal representations of VLMs can be achieved and used to repair model hallucinations and introduce new capabilities.

## 2 RELATED WORK

### 2.1 INTERPRETING LATENT REPRESENTATIONS IN LANGUAGE MODELS

Interpreting the inner workings of large language models enables fine-grained improvement of the language model behavior. Recent work involves utilizing the model’s attention maps (Kobayashi et al., 2020; Chefer et al., 2021), activation patterns (Conmy et al., 2023; Meng et al., 2023; Bronzini et al., 2024), and latent representations (Ghandeharioun et al., 2024; Cunningham et al., 2023; Bricken et al., 2023) to understand their behavior with applications such as early exiting (Halawi et al., 2024) and editing or erasing the model’s knowledge (Dai et al., 2022; Ravfogel et al., 2024). One class of methods probe the VLMs knowledge with linear classifiers (Hewitt & Manning, 2019; Tucker et al., 2021; Li et al., 2024; Belrose et al., 2023). The logit lens method (nostalgebraist, 2020), which we will use in our analysis, finds the output distribution over the vocabulary of the language model at intermediate layers with the model’s own unembedding matrix. We apply this approach to VLMs to interpret the model’s understanding of *visual information* in the model’s textual vocabulary.

### 2.2 INTERPRETING LATENT REPRESENTATIONS IN VISION MODELS

Understanding the internal dynamics of vision models is critical for ensuring safety and reliability in multimodal systems. Early works in this area focused on producing saliency maps (Petsiuk et al., 2018), analyzing individual neurons (Bau et al., 2020; 2019; Dravid et al., 2023), and training networks to map latent representations to concepts (Esser et al., 2020). With the emergence of transformer-based vision models like CLIP (Radford et al., 2021), recent methods explain latent tokens (Chen et al., 2023) and the roles of attention heads and neurons with natural language (Gandelsman et al., 2024b;a). Few works currently interpret the internal computation of VLMs: Palit et al. (2023) develop a neuron causal tracing tool; Schwettmann et al. (2023) identifies multi-modal neurons; and Huo et al. (2024) ablates domain-specific neurons to improve vision question-answering. Whereas past

papers have primarily studied the mechanisms (e.g. neuron analysis) that drive VLMs, we focus on interpreting and editing their latent representations for real-world applicability.

### 2.3 DETECTING AND REDUCING VLM HALLUCINATIONS

While VLM performances on image caption and visual question answering are continually improving, they continue to hallucinate facts that are not supported by the visual input. Existing methods for detecting hallucinations in language models during inference utilize latent representations (He et al., 2024; Su et al., 2024), activations (Chen et al., 2024), and output logit values (Varshney et al., 2023). SAPLMA (Azaria & Mitchell, 2023) trains a hallucination classifier on the internal latent representations. LUNA (Song et al., 2024) learns a transition function on latent representations and identifies abnormal transitions. Varshney et al. (2023) uses the final layer logits to score the model’s confidence in an entity or keyword and intervenes by instructing the model to either repair or remove the hallucinated information. Among VLMs, LURE (Zhou et al., 2024) is a fine-tuned revisor model to detect and reduce hallucinations. OPERA (Huang et al., 2024) uses the model’s internal attention weights to detect and suppress patterns that align with the beginning of hallucinated phrases. In contrast to these methods, we leverage the internal *image* representations in the VLMs for hallucination reduction and for zero-shot segmentation.

## 3 EXTRACTING KNOWLEDGE FROM VLMs

We start by introducing VLMs and the general framework of their architectures in most recent work. We then describe our approach for decoding the features in intermediate image representations in VLMs into text, and apply it to two types of VLMs. Surprisingly, this approach effectively probes the knowledge about objects present in images and can localize objects within the image.

### 3.1 PRELIMINARIES

**Vision-Language Models.** The architecture of recent state-of-the-art VLMs for text generation typically involves three main components: a vision encoder to process image inputs, a mapping network to map image features to image embeddings, and an autoregressive language model to process the image embeddings and prompt embeddings to generate text. We focus on two recent state-of-the-art VLMs: *LLaVA 1.5* (Liu et al., 2024a) and *InstructBLIP* (Dai et al., 2023). We use 7B versions of both these models. LLaVA utilizes a frozen CLIP vision encoder and an MLP as a mapping network to project the vision encoder outputs into image embeddings for the language model. The MLP is pre-trained on a large vision-language dataset and both the MLP and the language model are fine-tuned on an instruction-focused dataset. In contrast, InstructBLIP freezes both the vision encoder and the language model and only trains the mapping network.

**Notations.** For the purposes of our work, we define the VLM architecture as follows. The vision encoder processes an input image to produce  $n$  image features. These image features are projected to embedding space via the mapping network, resulting in  $n$   $d$ -dimensional image embeddings  $\{k_i : k_i \in \mathbb{R}^d, i = 1, \dots, n\}$ . For the language model, the entire set of text tokens constitutes the vocabulary  $V$  with vocabulary size  $|V|$ . The image embeddings, followed by  $m$  text embeddings  $\{t_i : t_i \in \mathbb{R}^d, i = 1, \dots, m\}$  of the prompt tokens, are input to the language model through  $L$  decoder layers. For an input embedding  $x \in \mathbb{R}^d$ , we define  $h_l(x) \in \mathbb{R}^d$  to be the latent representation for embedding  $x$  at layer  $l \in \{1, \dots, L\}$ , the output of the decoder layer, which is conditioned on previous tokens of the input sequence. An unembedding matrix  $W_U \in \mathbb{R}^{|V| \times d}$  maps the last latent representation  $h_L(t_m)$  to a probability distribution over the vocabulary for the next token  $t_{m+1}$ .

**Logit Lens.** Logit Lens is an interpretability method for intermediate language model representations introduced in Section 2.1. The logit lens technique applies the unembedding matrix  $W_U$  to latent representations  $h_l(x)$  in the  $L$  intermediate layers in the language model to retrieve the logit distributions over the vocabulary.

$$f_l(t_m) = W_U \cdot h_l(t_m) = [\text{logit}_1, \text{logit}_2, \text{logit}_3, \dots, \text{logit}_{|V|}] \quad (1)$$

This is the logit distribution representing the predictions of the model after  $l$  layers, where  $\text{logit}_j$  corresponds to the token  $j$  in the vocabulary.

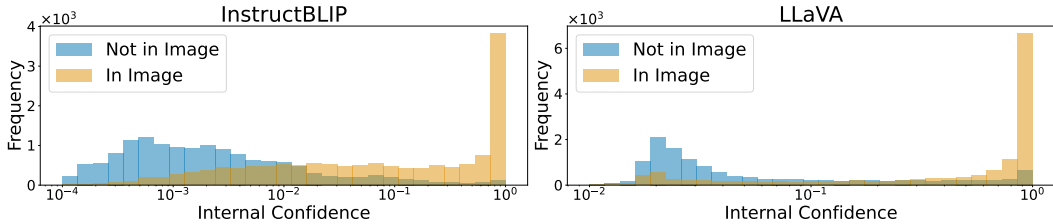


Figure 2: **Comparison of internal confidence in objects present and not present in the image.** We examine the internal confidence of COCO objects that exist and do not exist in the image within intermediate VLM image representations. We observe that objects that do not exist in the image have lower internal confidence.

### 3.2 APPLYING LOGIT LENS ON VLMS

We apply the logit lens to probe the language model as it processes the image representations. This enables us to interpret the image features’ output distributions as they are transformed by the layers of the language model and localize objects spatially within the image.

**Extracting probability distributions from intermediate image representations.** We apply logit lens on the *image representations* in the VLM. For a given image embedding  $k_i$ , we find the latent representation of the image embedding at layer  $l$ ,  $h_l(k_i)$ , taking the logit lens to get the probability distribution over the vocabulary,  $\text{softmax}(f_l(k_i))$ . We define an object  $o$ , an object word composed of tokens from the vocabulary. We inspect the probability of a specific object  $o$ ,  $\text{softmax}(f_l(k_i))_o$ . For multi-token objects, we take the maximum probability value over the object tokens. This provides a generalizable framework for analyzing specific latent image representations via text, with respect to specific objects. Next, we find the maximum probability over all image representations over all layers. For object  $o$ , we compute:

$$c_o = \max_{\substack{1 \leq l \leq L \\ 1 \leq i \leq n}} \{\text{softmax}(f_l(k_i))_o\} \quad (2)$$

We define  $c_o$  as the VLMs *internal confidence* of an object  $o$  existing in the image: the highest probability of object presence across  $n$  image representations through  $L$  layers of the language model.

**Comparing the internal confidence of present and not present objects.** To determine if internal confidence provides meaningful information about objects in the image, we examine  $c_o$  for objects present and not present in an image. We use InstructBLIP and LLaVA to caption 5000 random COCO2014 images in the Karpathy validation split (Lin et al., 2015) and determine  $c_o$  for all 80 COCO objects, only a few of which are present in each image. Since there are many more objects not present than present, we randomly sample a subset of the internal confidences for objects not present. Figure 2 exhibits the internal confidences for objects present and not present in the image. We empirically find that the VLMs’ internal confidences are higher for present objects than not present ones. We use this claim later to classify objects as hallucinations in Section 5.1.

**Object localization.** Given that the language model can distinguish between objects present and not present in an image, we examine whether it can attribute high object internal confidence to specific patches in an image. For each image embedding  $k_i$  in  $n$  image embeddings, we find the maximum softmax probability of an object within the layers of the model,  $\max_{1 \leq l \leq L} \{\text{softmax}(f_l(k_i))_o\}$ . Using these internal confidence values, we localize the objects in the image patches, each of which maps to an image embedding. We focus on LLaVA for this task, since its image encoder preserves the spatial mapping of image patches to image features.

We observe that image representations that exhibit higher internal confidence for specific objects correspond to the image patches in which those objects are visually present (examples in Figure 3). Building on our previous observation, we see that the intermediate image representations semantically align with latent token representations of objects present in them while maintaining their spatial locality. We use this unique finding for zero-shot segmentation in Section 5.3.

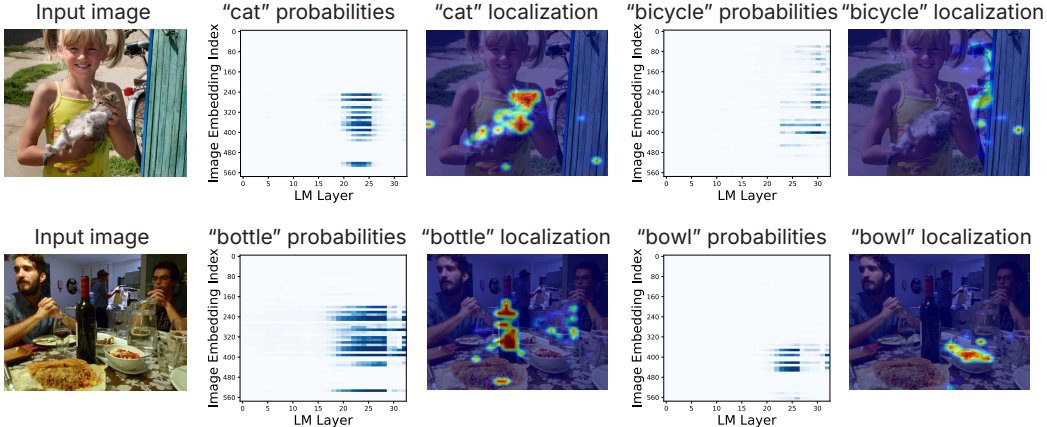


Figure 3: **Localizing objects using internal confidence values.** We find the probabilities of objects through layers of the language model for every image embedding in LLaVA. We use the highest layer probability per image embedding to localize an object within the image.

While the model is not directly trained to map the image representations closer to the text representations of objects within them, we can unembed the image representations in the text vocabulary for localization and find differences in internal confidence for present and hallucinated objects. In Section 5.1, we will use this observation for various applications including hallucination detection and zero-shot segmentation.

## 4 ERASING KNOWLEDGE FROM VLMS

Recognizing that image embeddings are directly interpretable (Section 3.2), we edit these embeddings to erase the presence of objects from image captions. We propose a linear editing algorithm that subtracts the text embedding of a target object from all image embeddings. When applied on singular and multiple object removals, we find that it erases hallucinated objects more effectively than correctly detected (CD) objects (i.e. real objects that the model correctly detects).

### 4.1 ERASING OBJECTS FROM IMAGE REPRESENTATIONS

We present an algorithm, PROJECTAWAY (Figure 4), that orthogonalizes image representations with respect to text representations in order to erase objects in image captions, applying it to remove objects one at a time and all at once.

Given an image and an object to remove, we edit the latent representations  $h_{l^I}(k_i)$  at a hidden layer  $l^I$  across all image embeddings  $k_i$ . We do not modify any latent representations outside of those belonging to image features. We compute the dot product,  $p$ , of  $h_{l^I}(k_i)$  and the object’s text embedding  $\vec{t}$ , subtracting a weighted  $\vec{t}$  from  $h_{l^I}(k_i)$  only if the dot product is positive. At  $\alpha = 1$ , PROJECTAWAY is equivalent to orthogonalizing the image representations with respect to the text representation. To compute text representation  $\vec{t}$ , we pass the object (e.g. “hot dog”) into the VLM’s text model and extract  $h_{l^T}(t_{-1})$  at hidden layer  $l^T$ , where  $t_{-1}$  is the last token of the object. We use the last token of the object to capture the whole of the object’s meaning.

Algorithm 1: PROJECTAWAY

---

**Input:** A set of image embeddings  $K$ , text embedding  $\vec{t}$ , and weight factor  $\alpha$   
**Output:** A set of modified image embeddings  $K'$  projected away from the text embedding  
**Initialization:**  $K' \leftarrow \emptyset$   
**for**  $\vec{k} \in K$  **do**  
     $p \leftarrow \vec{k} \cdot \vec{t}$   
    **if**  $p > 0$  **then**  
         $K' \leftarrow K' \cup \{\vec{k} - \alpha \cdot \frac{p}{\|\vec{t}\|_2} \cdot \vec{t}\}$   
    **else**  
         $K' \leftarrow K' \cup \{\vec{k}\}$   
    **end if**  
**end for**

---

Figure 4: Our editing algorithm erases the presence of an object from image embeddings by orthogonalizing them with respect to the object’s text embedding.

Edit Scope	Model	Individual RR (%)	Mass RR (%)	CD change (%)	$C_i \downarrow$	$C_s \downarrow$
No edits	InstructBLIP	-	-	-	15.0	54.1
	LLaVA	-	-	-	14.6	51.1
Hallucinations	InstructBLIP	83.3	74.3	+0.07	8.94	33.2
	LLaVA	86.0	72.8	+0.01	11.2	35.5
CD	InstructBLIP	16.2	15.0	-2.2	17.3	58.3
	LLaVA	6.9	8.3	-1.6	15.2	52.4

Table 1: **Removing mentioned objects individually & in-mass.** Using PROJECTAWAY, we remove hallucinated objects and observe high hallucination reduction with CHAIR, mass-removal rate (Mass RR), and individual removal rate (Individual RR). We also remove correctly detected (CD) objects but find that they are more resistant to linear editing. Denote CHAIR<sub>S</sub> as  $C_S$  and CHAIR<sub>I</sub> as  $C_I$ .

#### 4.1.1 REMOVING OBJECTS ONE BY ONE

We evaluate the PROJECTAWAY algorithm’s effectiveness at erasing individual objects from captions across multiple images and objects.

**Experimental setting.** We apply PROJECTAWAY on 5000 random images from the COCO2014 training set on all mentioned COCO objects (i.e. hallucination and CD) individually and measure the removal rate at which objects no longer appear in the caption. For InstructBLIP, we set  $(l^I, l^T, \alpha) = (1, 2, 1.5)$ . For LLaVA, we set  $(l^I, l^T, \alpha) = (19, 21, 3.5)$ . These parameters are fixed irrespective of image and are chosen for their maximal effect (see ablations in Section 4.2). To differentiate hallucinations from CD, we compute CHAIR (Rohrbach et al., 2019), an evaluation criteria that compares model-generated captions to ground-truth human annotations. CHAIR provides two main scores, CHAIR<sub>I</sub> and CHAIR<sub>S</sub>, that quantify hallucinations for instances and sentences, respectively:

$$\text{CHAIR}_S = \frac{|\{\text{captions with hallucinated objects}\}|}{|\{\text{all captions}\}|}, \text{CHAIR}_I = \frac{|\{\text{hallucinated objects}\}|}{|\{\text{all objects mentioned}\}|} \quad (3)$$

**Results.** Table 1 shows that PROJECTAWAY is significantly more effective in erasing individual hallucinated objects at an individual level than CD objects for both InstructBLIP and LLaVA. Along with the insight that hallucinated objects have lower softmax scores (Figure 2), these results suggest that hallucinated objects manifest more weakly in image embeddings and are hence easier to remove than CD objects.

#### 4.1.2 MASS-REMOVING OBJECTS

We iteratively apply PROJECTAWAY to a *set* of objects, following the same experimental setup and observing similarly different removal rates for hallucinated objects and CD objects.

**Mass-removing hallucinations.** We mass-remove hallucinations identified with ground truth annotations using PROJECTAWAY. Table 1 shows that editing out all the hallucinations of an image yields a similar removal rate as individually editing out and, importantly, that erasing hallucinated objects together does not interfere with each other. We achieve a hallucination reduction rate of 41.3% for InstructBLIP and 23.3% for LLaVA (see Table 4). Recall count slightly *increases* for both models, indicating that caption accuracy is preserved. This may be because removed hallucinations are replaced with objects the model is more confident in. Qualitative results are in Figure 5.

**Mass removing CD.** We similarly find that applying PROJECTAWAY can successfully remove CD objects when edited all together in Table 1. Furthermore, CHAIR scores minimally change, which indicates that this mass-removal merely erases object presence without eroding caption accuracy. While the removal rate is lower than for hallucinated objects, this insight proves useful when we apply PROJECTAWAY for hallucination reduction in Section 5.2.

## 4.2 ABLATION STUDY: MASS-REMOVING HALLUCINATIONS

We perform ablations on parameters of PROJECTAWAY to improve object removal rate for erasing hallucinations in-mass.



Figure 5: **Qualitative results for mass object removal.** We present example images and their captions after mass-removing hallucinations (red) with PROJECTAWAY., which can effectively remove hallucinations while preserving, even increasing, correctly detected objects (green).

**Experimental setting.** We ablate the three parameters of PROJECTAWAY: layer  $l^I$  to edit at, layer  $l^T$  to retrieve the text representation, and weight factor  $\alpha$ . At  $l^T = -1$ , we average together the object’s constituent token embeddings. At  $l^I = -1$ , we edit the image embeddings directly inputted to the text model. We evaluate across 500 training samples from COCO 2014 that have at least one hallucination.

**Hidden layers.** Figure 6 shows hallucination reduction rate on LLaVA from mass-removing hallucinations on every combination of  $l^I$  and  $l^T$  (each from -1 to 31). As a core concern is that editing erodes caption accuracy, we gray out any combination that reduces CD objects. For InstructBLIP (see Figure 10), the best parameters ( $l^I = 1, l^T = 2$ ) reduces hallucinations by 38.5%. For LLaVA, our best parameters ( $l^I = 19, l^T = 21$ ) reduce hallucinations by 25.7%, and the middle layers are the best to edit and extract latent text embeddings from. Our results also provide a wide range of reasonable parameter alternatives to use if this reduction rate does not generalize beyond our samples.

**Weight factor.** Using the best-reduced hidden layers, we ablate the weight factor  $\alpha$  for PROJECTAWAY across the same 500 randomly selected COCO images. Figure 7 shows that as  $\alpha$  increases, hallucinations are removed at a higher rate, and the overall hallucination count drops significantly. At high  $\alpha$ , we observe through anecdotal examples that captions become nonsensical, as quantitatively shown by the complete loss of both correctly detected and hallucinated objects from the caption. Therefore, as a pre-caution, we only select weight factors that do not reduce CD objects when we apply PROJECTAWAY to erase hallucinated objects.

## 5 APPLICATIONS

### 5.1 HALLUCINATION DETECTION

When extracting knowledge from VLMs in Section 3.2, we found that applying logit lens on in-context image representations exhibit useful information about visual objects present in the image. Using these observations, we present an approach for object presence classification that only relies on the VLMs own parameters. We utilize the internal confidence  $c_o$  value to classify object presence,

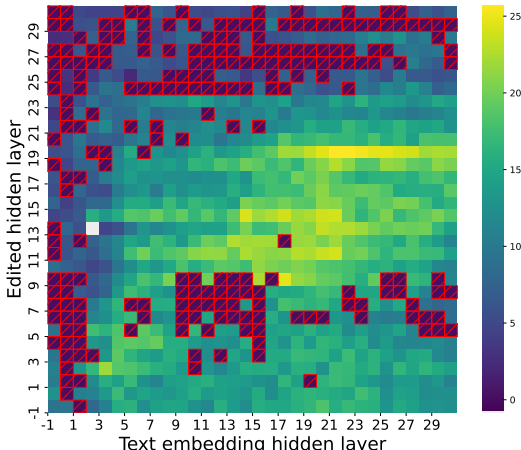


Figure 6: **Hidden layer ablations** for LLaVA. We track hallucination reduction (%) across different layers to edit at and extract latent embeddings for the text embedding, crossing out (red) parameters from consideration where there is a decrease in correctly detected objects.

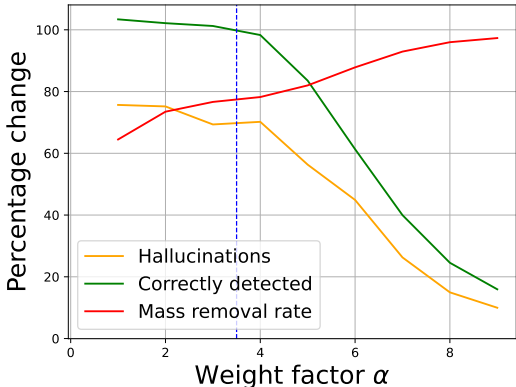


Figure 7: **Weight ablations** for LLaVA. We vary the weight factor  $\alpha$  and measure changes in correctly detected objects, removal rate, and hallucination reduction. We observe a decline in hallucinations as weight grows and mark a weight where there is no loss in correctly detected objects.

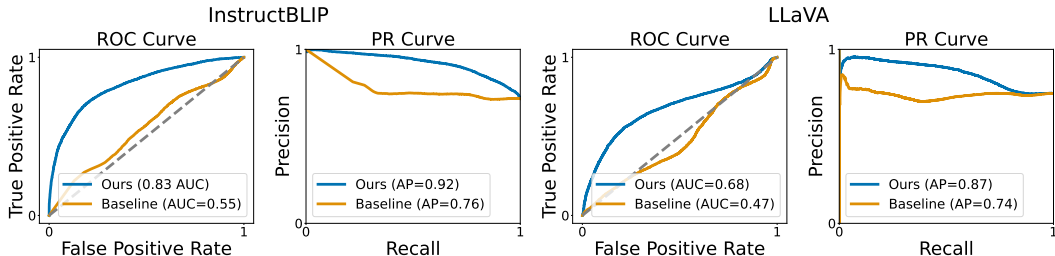


Figure 8: **Object Presence Classification Curves for InstructBLIP and LLaVA.** We show the Precision-Recall and ROC curves of our confidence measure for present object-hallucination classification on the COCO training subset. Classifying object presence with the internal confidence outperforms the baseline, indicating that the language model’s image representations know which objects are hallucinations and which are truly present.

since the internal confidence for objects that are not present in the image, or hallucinated, are lower within the image representations.

**Experimental setting.** We evaluate the strength of the internal confidence  $c_o$  as an indicator of object presence. We sample 5000 images from the MSCOCO training set, using the image captioning objective to caption methods with both InstructBLIP and LLaVA. We use the  $c_o$  for present objects and hallucinations within the captions generated by each VLM. We assess how well the internal confidence aligns with the ground truth labels of object presence, where a negative sample is a hallucination and a positive sample is a present object.

**Baseline.** As a baseline, we use the maximum output probability of the object’s tokens. This is the confidence of the model prediction. Previous works such as Zhou et al. (2024) have found that hallucinations occur more frequently on objects characterized by high uncertainty during generation.

**Results.** We present quantitative results in Figure 8 and Table 5. We show qualitative results for LLaVA (Figure 14) and InstructBLIP (Figure 15) in the Appendix. We find that utilizing internal confidence to classify object hallucinations provides a 47.17% improvement in mAP in InstructBLIP and 22.45% in LLaVA. Furthermore, the ROC AUC improves over the baseline by 50.10% in InstructBLIP and 44.68% in LLaVA, indicating stronger object presence classification.



Model	Method	CHAIR <sub>i</sub> ↓	CHAIR <sub>s</sub> ↓	Hallucinated Objects ↓
InstructBLIP	Greedy	57.0	23.3	512
	Nucleus	58.0	24.0	508
	Beam Search	53.4	14.6	564
	OPERA	45.6	13.9	472
	Ours	<b>43.8</b>	<b>12.5</b>	<b>419</b>
LLaVA	Greedy	49.2	14.2	532
	Nucleus	55.8	17.1	618
	Beam Search	52.4	15.0	583
	OPERA	44.8	12.8	462
	Ours	<b>42.0</b>	<b>12.2</b>	<b>444</b>

Table 2: **Hallucination intervention performance.** We mass-remove hallucinations detected by the method in Section 5.1 and outperform other baselines. We observe a considerable drop in the raw count of hallucinated objects.

## 5.2 HALLUCINATION REMOVAL

We use the mass editing technique to remove hallucinations detected by the prior method. Section 4.1.2 successfully removes a significant portion of hallucinations but presupposes a knowledge of what the hallucinations are. We threshold on the internal confidence of each object to identify hallucinations and mass-remove them using PROJECTAWAY. Our chosen threshold prioritizes precision over recall (i.e. we allow classification of some CD objects as hallucinations) because CD objects are less affected by the removal method, as shown in Section 4.1.2.

**Experimental setting.** We threshold hallucinations as  $c_o < 0.2$  for InstructBLIP and  $c_o < 0.1$  for LLaVA. Based on prior ablations (Section 4.2), we select ( $l^I = 1, l^T = 2, \alpha = 1.5$ ) for InstructBLIP and ( $l^I = 19, l^T = 21, \alpha = 3.5$ ) for LLaVA. Our prompt is “Please describe this image in detail.”

**Baselines.** Since our method intervenes during the decoder step, we compare our method with 3 standard decoding algorithms. Greedy decoding predicts the next token based on the highest logit probability. Beam search maintains a tree of beams and selects the best beam at generation end. Nucleus sampling selects the next token from a set of high probability tokens whose cumulative probability reaches a threshold  $p$ . We also evaluate against OPERA (Huang et al., 2024), which mitigates hallucinations by adding an overtrust penalty during decoder generation. We set  $p = 0.9$  for nucleus sampling. We use beam search in our method and unify  $N_{\text{beam}} = 5$  for the baseline.

**Results.** We apply these parameters to 500 COCO images from the Karpathy validation set. We provide qualitative results in Figure 17 and Figure 16. Quantitative results in Table 2 show that we outperform our baselines and reduce hallucinations by 25.7% on InstructBLIP and 23.8% on LLaVA compared to beam search. Our approach achieves a similar hallucination reduction rate as Section 4.1.2, despite not precisely differentiating hallucinations and some CD objects being incorrectly edited out. Notably, our method relies on no training or external models, effectively offering a “free lunch.” We find similar performance on additional models (Appendix A.5) and attribute hallucinations (Appendix A.7).

## 5.3 ZERO-SHOT SEGMENTATION

Building upon our findings in Section 3.2, we utilize the internal confidence per image feature for zero-shot image segmentation. This application leverages the spatial information encoded in the image representations and demonstrates how VLMs internally represent and localize objects within images.

**Method.** Our approach leverages the spatial correspondence between image patches and their associated image embeddings. We use LLaVA to generate the name of the class in the image and we focus on the internal confidence of that class per image patch. We take the mean internal confidence for tokens comprising a class word. We resize the set of  $24 \times 24$  internal confidence values per image patch back into a fixed image size of  $336 \times 366$  pixels. We then apply a threshold to these confidence values to binarize them into a foreground/background segmentation for the object in the image.

Model	Method	Pixel Acc. $\uparrow$	mIoU $\uparrow$	mAP $\uparrow$
raw attention (CLIP)	Image Encoder	69.81	45.19	77.30
TextSpan (Gandelsman et al., 2024b)	Image Encoder	<u>75.57</u>	<u>53.60</u>	<b>80.22</b>
raw attention (VLM)	VLM	67.28	39.27	73.96
Ours	VLM	<b>76.16</b>	<b>54.26</b>	<u>79.90</u>

Table 3: **Segmentation Performance on ImageNet-segmentation.** Localizing objects using their probabilities within the image representations results in more accurate zero-shot segmentation than previous methods relying on vision encoders and VLMs.

**Baseline.** As a baseline, we extract the attention values of generated tokens with the image embeddings from LLaVA. We also compare to the segmentation method introduced by Gandelsman et al. (2024b), which utilizes the attention heads of the image encoder without the additional VLM processing, using the same image encoder (CLIP-ViT-L/14 at 336px).

**Results.** We evaluate our method on the Imagenet validation set. Qualitative results are shown in Figure 9 and quantitative comparisons with the baselines in Section 5.3. We improve mAP by 8.03% over using the VLMs raw attention values and provide better and/or comparable performance to other state-of-the-art methods that utilize just the image encoder. While the VLM is not directly trained for segmentation, our technique reveals that it still encodes significant *spatial* information about objects within its intermediate image representations.

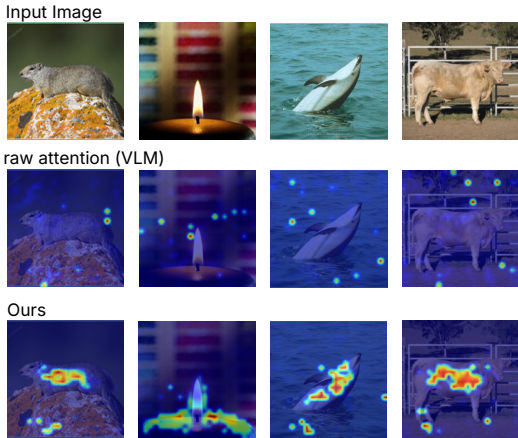


Figure 9: **Zero-shot segmentation.** Warmer areas indicate higher internal confidence for the class at that image patch. We binarize these values with a threshold to generate segmentations.

## 6 DISCUSSION AND LIMITATIONS

We interpreted VLMs’ image representations through the language model layers and discovered that linear editing of these representations can selectively remove object information via a simple orthogonalization. Our findings enabled hallucination reduction and improved zero-shot segmentation. We present two limitations of our work and conclude with future directions.

**Multi-token objects.** Our method simplifies the use of object words that may be composed of multiple tokens, such as by taking the max internal confidence over object tokens or utilizing the average token embedding for editing. This can introduce noise to the internal confidence if certain tokens are common in multiple different words and lead to an approximation of the object’s latent representations when editing.

**Fine-grained edits.** The editing approach may struggle with highly abstract or longer sentences that involve attributes or interactions of objects. Removing a full sentence, for example, is not something we assessed in this paper, since our focus is on the removal of individual objects.

**Future work.** While our focus was on interpreting objects and object hallucinations in VLMs, we believe that our approach can be extended to other key elements of visual scenes, such as people, attributes, and actions. We also focused on object removal, but we believe that editing can also be extended to inject objects into a caption (by adding instead of subtracting the text embedding). We hope to explore the applications of our approach in other multimodal architectures. Our insights may help design better VLMs that are more robust to hallucinations and have improved spatial understanding. We plan to explore these directions in our future work.

## 6.1 ACKNOWLEDGMENTS

We thank Kayo Yin for her comments and feedback on our paper. YG is supported by the Google Fellowship. Authors, as part of their affiliation with UC Berkeley, were supported in part by the Berkeley Artificial Intelligence Research (BAIR) commons program.

## REFERENCES

- Amos Azaria and Tom Mitchell. The internal state of an LLM knows when it’s lying. In Houda Bouamor, Juan Pino, and Kalika Bali (eds.), *Findings of the Association for Computational Linguistics: EMNLP 2023*, pp. 967–976, Singapore, December 2023. Association for Computational Linguistics. doi: 10.18653/v1/2023.findings-emnlp.68. URL <https://aclanthology.org/2023.findings-emnlp.68>.
- Jinze Bai, Shuai Bai, Shusheng Yang, Shijie Wang, Sinan Tan, Peng Wang, Junyang Lin, Chang Zhou, and Jingren Zhou. Qwen-vl: A versatile vision-language model for understanding, localization, text reading, and beyond, 2023. URL <https://arxiv.org/abs/2308.12966>.
- David Bau, Jun-Yan Zhu, Hendrik Strobelt, Bolei Zhou, Joshua B. Tenenbaum, William T. Freeman, and Antonio Torralba. Gan dissection: Visualizing and understanding generative adversarial networks. In *Proceedings of the International Conference on Learning Representations (ICLR)*, 2019.
- David Bau, Jun-Yan Zhu, Hendrik Strobelt, Agata Lapedriza, Bolei Zhou, and Antonio Torralba. Understanding the role of individual units in a deep neural network. *Proceedings of the National Academy of Sciences*, 2020. ISSN 0027-8424. doi: 10.1073/pnas.1907375117. URL <https://www.pnas.org/content/early/2020/08/31/1907375117>.
- Nora Belrose, Zach Furman, Logan Smith, Danny Halawi, Igor Ostrovsky, Lev McKinney, Stella Biderman, and Jacob Steinhardt. Eliciting latent predictions from transformers with the tuned lens, 2023. URL <https://arxiv.org/abs/2303.08112>.
- Trenton Bricken, Adly Templeton, Joshua Batson, Brian Chen, Adam Jermyn, Tom Conerly, Nick Turner, Cem Anil, Carson Denison, Amanda Askell, Robert Lasenby, Yifan Wu, Shauna Kravec, Nicholas Schiefer, Tim Maxwell, Nicholas Joseph, Zac Hatfield-Dodds, Alex Tamkin, Karina Nguyen, Brayden McLean, Josiah E Burke, Tristan Hume, Shan Carter, Tom Henighan, and Christopher Olah. Towards monosemanticity: Decomposing language models with dictionary learning. Transformer Circuits Thread, 2023. URL <https://transformer-circuits.pub/2023/monosemantic-features/index.html>.
- Marco Bronzini, Carlo Nicolini, Bruno Lepri, Jacopo Staiano, and Andrea Passerini. Unveiling llms: The evolution of latent representations in a dynamic knowledge graph, 2024. URL <https://arxiv.org/abs/2404.03623>.
- Hila Chefer, Shir Gur, and Lior Wolf. Generic attention-model explainability for interpreting bi-modal and encoder-decoder transformers, 2021. URL <https://arxiv.org/abs/2103.15679>.
- Chao Chen, Kai Liu, Ze Chen, Yi Gu, Yue Wu, Mingyuan Tao, Zhihang Fu, and Jieping Ye. Inside: LLMs’ internal states retain the power of hallucination detection, 2024. URL <https://arxiv.org/abs/2402.03744>.
- Haozhe Chen, Junfeng Yang, Carl Vondrick, and Chengzhi Mao. Interpreting and controlling vision foundation models via text explanations, 2023. URL <https://arxiv.org/pdf/2310.10591>.
- Arthur Conmy, Augustine N. Mavor-Parker, Aengus Lynch, Stefan Heimersheim, and Adrià Garriga-Alonso. Towards automated circuit discovery for mechanistic interpretability, 2023. URL <https://arxiv.org/abs/2304.14997>.
- Hoagy Cunningham, Aidan Ewart, Logan Riggs, Robert Huben, and Lee Sharkey. Sparse autoencoders find highly interpretable features in language models, 2023. URL <https://arxiv.org/abs/2309.08600>.

- Damai Dai, Li Dong, Yaru Hao, Zhifang Sui, Baobao Chang, and Furu Wei. Knowledge neurons in pretrained transformers, 2022. URL <https://arxiv.org/abs/2104.08696>.
- Wenliang Dai, Junnan Li, Dongxu Li, Anthony Meng Huat Tiong, Junqi Zhao, Weisheng Wang, Boyang Li, Pascale Fung, and Steven Hoi. Instructblip: Towards general-purpose vision-language models with instruction tuning, 2023. URL <https://arxiv.org/abs/2305.06500>.
- Amil Dravid, Yossi Gandelsman, Alexei A. Efros, and Assaf Shocher. Rosetta neurons: Mining the common units in a model zoo. In *Proceedings of the IEEE/CVF International Conference on Computer Vision (ICCV)*, pp. 1934–1943, October 2023.
- Patrick Esser, Robin Rombach, and Bjorn Ommer. A disentangling invertible interpretation network for explaining latent representations, 2020. URL <https://arxiv.org/pdf/2004.13166>.
- Yossi Gandelsman, Alexei A. Efros, and Jacob Steinhardt. Interpreting the second-order effects of neurons in clip, 2024a. URL <https://arxiv.org/abs/2406.04341>.
- Yossi Gandelsman, Alexei A. Efros, and Jacob Steinhardt. Interpreting clip’s image representation via text-based decomposition, 2024b. URL <https://arxiv.org/pdf/2310.05916>.
- Asma Ghandeharioun, Avi Caciularu, Adam Pearce, Lucas Dixon, and Mor Geva. Patchscopes: A unifying framework for inspecting hidden representations of language models, 2024. URL <https://arxiv.org/abs/2401.06102>.
- Danny Halawi, Jean-Stanislas Denain, and Jacob Steinhardt. Overthinking the truth: Understanding how language models process false demonstrations, 2024. URL <https://arxiv.org/abs/2307.09476>.
- Jinwen He, Yujia Gong, Kai Chen, Zijin Lin, Chengan Wei, and Yue Zhao. Llm factoscope: Uncovering llms’ factual discernment through inner states analysis, 2024. URL <https://arxiv.org/abs/2312.16374>.
- John Hewitt and Christopher D. Manning. A structural probe for finding syntax in word representations. In Jill Burstein, Christy Doran, and Thamar Solorio (eds.), *Proceedings of the 2019 Conference of the North American Chapter of the Association for Computational Linguistics: Human Language Technologies, Volume 1 (Long and Short Papers)*, pp. 4129–4138, Minneapolis, Minnesota, June 2019. Association for Computational Linguistics. doi: 10.18653/v1/N19-1419. URL <https://aclanthology.org/N19-1419>.
- Yuan Hu, Jianlong Yuan, Congcong Wen, Xiaonan Lu, and Xiang Li. Rsgpt: A remote sensing vision language model and benchmark, 2023. URL <https://arxiv.org/abs/2307.15266>.
- Qidong Huang, Xiaoyi Dong, Pan Zhang, Bin Wang, Conghui He, Jiaqi Wang, Dahua Lin, Weiming Zhang, and Nenghai Yu. Opera: Alleviating hallucination in multi-modal large language models via over-trust penalty and retrospection-allocation, 2024. URL <https://arxiv.org/abs/2311.17911>.
- Jiahao Huo, Yibo Yan, Boren Hu, Yutao Yue, and Xuming Hu. Mmneuron: Discovering neuron-level domain-specific interpretation in multimodal large language model, 2024. URL <https://arxiv.org/pdf/2406.11193v1>.
- Ziwei Ji, Nayeon Lee, Rita Frieske, Tiezheng Yu, Dan Su, Yan Xu, Etsuko Ishii, Ye Jin Bang, Andrea Madotto, and Pascale Fung. Survey of hallucination in natural language generation. *ACM Computing Surveys*, 55(12):1–38, March 2023. ISSN 1557-7341. doi: 10.1145/3571730. URL <http://dx.doi.org/10.1145/3571730>.
- Goro Kobayashi, Tatsuki Kuribayashi, Sho Yokoi, and Kentaro Inui. Attention is not only a weight: Analyzing transformers with vector norms. In Bonnie Webber, Trevor Cohn, Yulan He, and Yang Liu (eds.), *Proceedings of the 2020 Conference on Empirical Methods in Natural Language Processing (EMNLP)*, pp. 7057–7075, Online, November 2020. Association for Computational Linguistics. doi: 10.18653/v1/2020.emnlp-main.574. URL <https://aclanthology.org/2020.emnlp-main.574>.

- Junnan Li, Dongxu Li, Silvio Savarese, and Steven Hoi. Blip-2: Bootstrapping language-image pre-training with frozen image encoders and large language models, 2023a. URL <https://arxiv.org/abs/2301.12597>.
- Kenneth Li, Aspen K. Hopkins, David Bau, Fernanda Viégas, Hanspeter Pfister, and Martin Wattenberg. Emergent world representations: Exploring a sequence model trained on a synthetic task, 2024. URL <https://arxiv.org/abs/2210.13382>.
- Yifan Li, Yifan Du, Kun Zhou, Jinpeng Wang, Wayne Xin Zhao, and Ji-Rong Wen. Evaluating object hallucination in large vision-language models, 2023b. URL <https://arxiv.org/abs/2305.10355>.
- Tsung-Yi Lin, Michael Maire, Serge Belongie, Lubomir Bourdev, Ross Girshick, James Hays, Pietro Perona, Deva Ramanan, C. Lawrence Zitnick, and Piotr Dollár. Microsoft coco: Common objects in context, 2015. URL <https://arxiv.org/abs/1405.0312>.
- Haotian Liu, Chunyuan Li, Yuheng Li, and Yong Jae Lee. Improved baselines with visual instruction tuning, 2024a. URL <https://arxiv.org/abs/2310.03744>.
- Haotian Liu, Chunyuan Li, Yuheng Li, Bo Li, Yuanhan Zhang, Sheng Shen, and Yong Jae Lee. Llava-next: Improved reasoning, ocr, and world knowledge, January 2024b. URL <https://llava-vl.github.io/blog/2024-01-30-llava-next/>.
- Fuwen Luo, Chi Chen, Zihao Wan, Zhaolu Kang, Qidong Yan, Yingjie Li, Xiaolong Wang, Siyu Wang, Ziyue Wang, Xiaoyue Mi, Peng Li, Ning Ma, Maosong Sun, and Yang Liu. Codis: Benchmarking context-dependent visual comprehension for multimodal large language models, 2024. URL <https://arxiv.org/abs/2402.13607>.
- Kevin Meng, David Bau, Alex Andonian, and Yonatan Belinkov. Locating and editing factual associations in gpt, 2023. URL <https://arxiv.org/abs/2202.05262>.
- nostalgebraist. Interpreting GPT: The logit lens. LessWrong, Aug 2020. URL <https://www.lesswrong.com/posts/AcKRB8wDpdaN6v6ru/interpreting-gpt-the-logit-lens>.
- Vedant Palit, Rohan Pandey, Aryaman Arora, and Paul Pu Liang. Towards vision-language mechanistic interpretability: A causal tracing tool for blip, 2023. URL <https://arxiv.org/pdf/2308.14179>.
- Vitali Petsiuk, Abir Das, and Kate Saenko. Rise: Randomized input sampling for explanation of black-box models, 2018. URL <https://arxiv.org/pdf/1806.07421>.
- Alec Radford, Jong Wook Kim, Chris Hallacy, Aditya Ramesh, Gabriel Goh, Sandhini Agarwal, Girish Sastry, Amanda Askell, Pamela Mishkin, Jack Clark, Gretchen Krueger, and Ilya Sutskever. Learning transferable visual models from natural language supervision, 2021. URL <https://arxiv.org/pdf/2103.00020>.
- Shauli Ravfogel, Michael Twiton, Yoav Goldberg, and Ryan Cotterell. Linear adversarial concept erasure, 2024. URL <https://arxiv.org/abs/2201.12091>.
- Anna Rohrbach, Lisa Anne Hendricks, Kaylee Burns, Trevor Darrell, and Kate Saenko. Object hallucination in image captioning, 2019. URL <https://arxiv.org/abs/1809.02156>.
- Sarah Schwettmann, Neil Chowdhury, Samuel Klein, and Antonio Torralba. Multimodal neurons in pretrained text-only transformers, 2023. URL <https://arxiv.org/pdf/2308.01544>.
- Da Song, Xuan Xie, Jiayang Song, Derui Zhu, Yuheng Huang, Felix Juefei-Xu, and Lei Ma. Luna: A model-based universal analysis framework for large language models, 2024. URL <https://arxiv.org/abs/2310.14211>.
- Weihang Su, Changyue Wang, Qingyao Ai, Yiran HU, Zhijing Wu, Yujia Zhou, and Yiqun Liu. Unsupervised real-time hallucination detection based on the internal states of large language models, 2024. URL <https://arxiv.org/abs/2403.06448>.

- Shengbang Tong, Ellis Brown, Penghao Wu, Sanghyun Woo, Manoj Middepogu, Sai Charitha Akula, Jihan Yang, Shusheng Yang, Adithya Iyer, Xichen Pan, Austin Wang, Rob Fergus, Yann LeCun, and Saining Xie. Cambrian-1: A fully open, vision-centric exploration of multimodal llms, 2024. URL <https://arxiv.org/abs/2406.16860>.
- Mycal Tucker, Peng Qian, and Roger Levy. What if this modified that? syntactic interventions via counterfactual embeddings, 2021. URL <https://arxiv.org/abs/2105.14002>.
- Neeraj Varshney, Wenlin Yao, Hongming Zhang, Jianshu Chen, and Dong Yu. A stitch in time saves nine: Detecting and mitigating hallucinations of llms by validating low-confidence generation, 2023. URL <https://arxiv.org/abs/2307.03987>.
- Dimitri von Rutte, Sotiris Anagnostidis, Gregor Bachmann, and Thomas Hofmann. A language model’s guide through latent space, 2024. URL <https://arxiv.org/pdf/2402.14433>.
- Qinghao Ye, Haiyang Xu, Jiabo Ye, Ming Yan, Anwen Hu, Haowei Liu, Qi Qian, Ji Zhang, Fei Huang, and Jingren Zhou. mplug-owl2: Revolutionizing multi-modal large language model with modality collaboration, 2023. URL <https://arxiv.org/abs/2311.04257>.
- Shukang Yin, Chaoyou Fu, Sirui Zhao, Tong Xu, Hao Wang, Dianbo Sui, Yunhang Shen, Ke Li, Xing Sun, and Enhong Chen. Woodpecker: Hallucination correction for multimodal large language models, 2023. URL <https://arxiv.org/abs/2310.16045>.
- Jinrui Zhang, Teng Wang, Haigang Zhang, Ping Lu, and Feng Zheng. Reflective instruction tuning: Mitigating hallucinations in large vision-language models, 2024a. URL <https://arxiv.org/abs/2407.11422>.
- Shaolei Zhang, Tian Yu, and Yang Feng. Truthx: Alleviating hallucinations by editing large language models in truthful space, 2024b. URL <https://arxiv.org/pdf/2402.17811>.
- Yiyang Zhou, Chenhong Cui, Jaehong Yoon, Linjun Zhang, Zhun Deng, Chelsea Finn, Mohit Bansal, and Huaxiu Yao. Analyzing and mitigating object hallucination in large vision-language models, 2024. URL <https://arxiv.org/abs/2310.00754>.

Edit Scope	Model	Hallucinations	CD
No edits	InstructBLIP	4545	14178
	LLaVA	4372	15053
Hallucinations	InstructBLIP	2672	14189
	LLaVA	3348	15061
CD	InstructBLIP	5078	13864
	LLaVA	4583	14826

Table 4: **Supplemental metrics for Table 1.** We measure unique hallucinated and correctly detected (CD) objects.

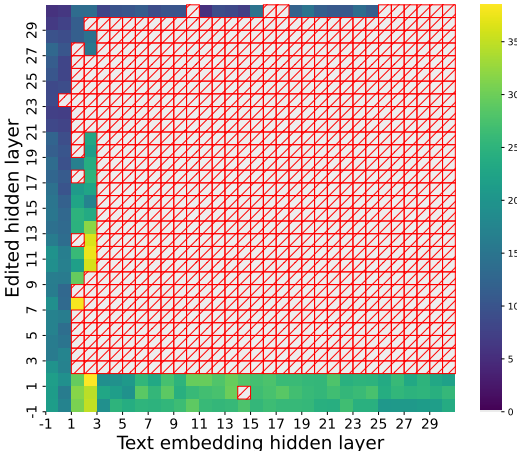


Figure 10: **Hidden layer ablations for InstructBLIP.** We track hallucination reduction (%) across different layers to edit at and extract latent embeddings for the text embedding, crossing out (red) parameters from consideration where there is a decrease in correctly detected objects.

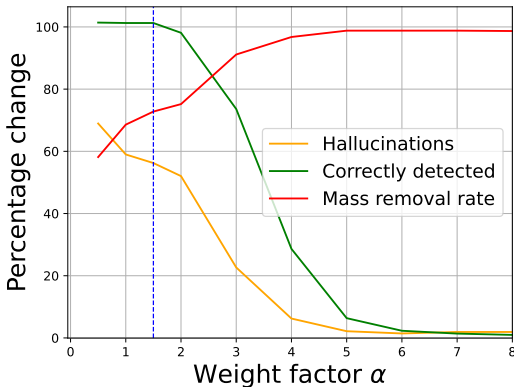


Figure 11: **Weight ablations for InstructBLIP.** We vary the weight factor  $\alpha$  and measure changes in correctly detected objects, object removal rate, and hallucination reduction. We observe a decline in hallucinations as weight increases and mark a weight where there is no loss in correctly detected objects.

## A APPENDIX

### A.1 MASS-REMOVING OBJECTS

We mass-remove mentioned objects (hallucinations and correctly detected) with PROJECTAWAY and tally up the total number of unique hallucinated and CD objects in Table 4.

### A.2 ABLATIONS FOR INSTRUCTBLIP

We show hidden layer and weight ablations for mass-removing hallucinations in InstructBLIP referenced in Section 4.2. The hidden layer ablations indicate that most of the parameter space is too sensitive to edit and leads to losses in correctly detected objects. We find that smaller  $l^T$  and  $l^I$  parameters are the most effective for reducing hallucinations. Our best parameters ( $l^I = 1, l^T = 2$ ) reduce hallucinations by 38.5%. It is not fully understood why the majority of the parameter search space is invalid in comparison with LLaVA in Figure 6. It is possible that the fine-tuning step in LLaVA semantically aligns hidden image representations with text embeddings more than InstructBLIP, allowing linear edits to have the precise, intended effect.

### A.3 HALLUCINATION DETECTION

We show quantitative comparisons from our hallucination detection approach using internal confidence (Section 5.1) to the baseline in Table 5. We also show qualitative examples for LLaVA in Figure 14 and for InstructBLIP in Figure 15. These samples exhibit model-generated captions, parsed objects, and whether they are classified as hallucinated or correctly detected based on their internal confidence score.

### A.4 HALLUCINATION REDUCTION

We exhibit sample results from our hallucination reduction approach (Section 5.2), which linearly removes text representations of hallucinations from image representations, in Figure 17 for InstructBLIP and Figure 16 for LLaVA. We show the image caption before and after our linear editing method, removing objects detected as hallucinations.

### A.5 QUANTITATIVE EVALUATIONS ON MORE ADVANCED MODELS

We evaluate our approach on two additional models, LLaVA-NeXT 7B (Liu et al., 2024b) and Cambrian-1 8B (Tong et al., 2024) with Llama 3. We threshold hallucinations as  $c_o < 0.4$  for LLaVA-NeXT and  $c_o < 0.3$  for Cambrian-1. Based on qualitative examples and referencing optimal parameters from other models in Section 4.2, we select ( $l^I = 24, l^T = 22, \alpha = 2$ ) for both models. We show quantitative results for hallucination detection in Table 6 and for hallucination intervention in Table 7. With our method, we observe a 27.73% improvement in CHAIR<sub>S</sub> with LLaVA-NeXT and a 28.86% improvement with Cambrian-1, demonstrating consistency with our findings on the LLaVA and InstructBLIP models.

### A.6 OBJECT LOCALIZATION

We show qualitative examples for localization with internal confidence for specific image representations, specifically for the LLaVA model, in Figure 18.

### A.7 ATTRIBUTE HALLUCINATIONS

Our analysis in this paper centered on object hallucinations because automated tooling and benchmarks for attribute (ex. shape, color, number) hallucinations are relatively sparse. However, we demonstrate the applicability of our editing technique on attribute hallucinations with qualitative examples filtered from the VQA 2.0 challenge in Figure 12. We reuse the editing hyperparameters for InstructBLIP ( $l_I = 1, l_T = 2, \alpha = 1.5$ ) and only edit attributes with  $c_o < 0.05$ .

### A.8 ZERO-SHOT CLASSIFICATION

We evaluate the strength of internal confidence derived from the logit lens on image representations for classification of the COCO class within patches of the image. We use the COCO ground truth segmentations to find ground truth classes for image patches. We determine the accuracy of the rankings found from logit lens internal confidence scores to predict the class per patch and present our results in Table 8. We find that these values highly vary across classes, which we hypothesize is because certain classes such as “person” are represented with more specific tokens such as “doctor”, “skier”, “girl”, etc. resulting in lower internal confidence for the tokens in “person” while other objects like “toothbrush”, “banana”, and “broccoli” are described in the same word as the COCO class.

### A.9 QUALITATIVE EXAMPLES BEYOND COCO 2014

We focus on COCO 2014 in our analyses because CHAIR, our main evaluation criteria, is tied with the dataset and can automatically categorize objects of interest in image captions. While COCO 2014 is a diverse set of images, we provide qualitative examples of hallucination reduction (see Section 5.2) on images from LLaVA-Bench (Liu et al., 2024b), a collection of 24 images of varying subjects. The examples in Figure 13 using InstructBLIP align with the strong hallucination reduction observed with COCO 2014.



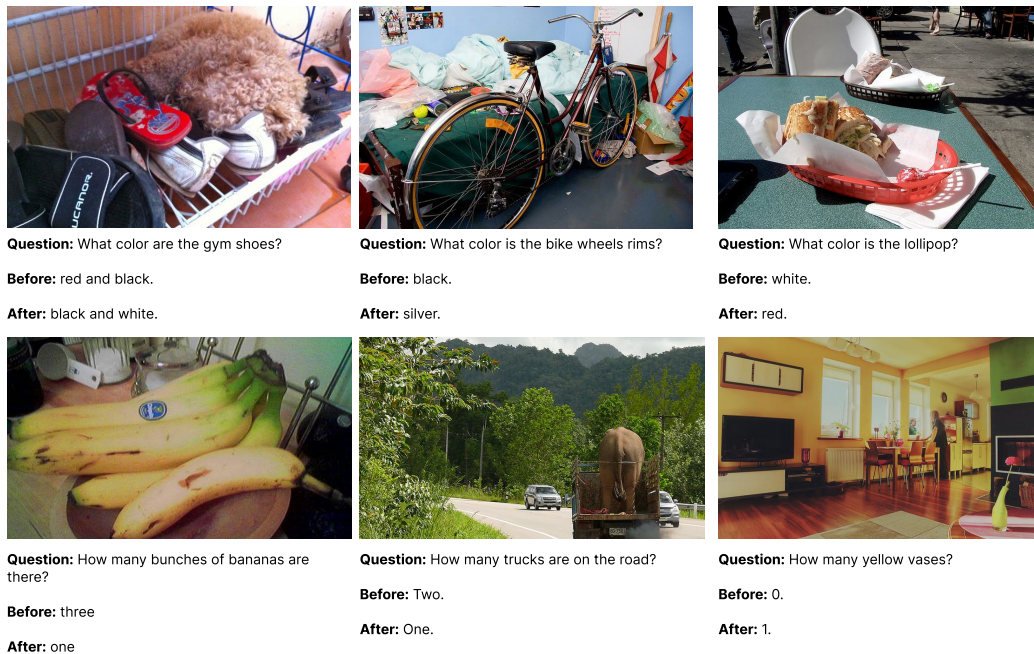


Figure 12: **Qualitative results for attribute hallucinations using InstructBLIP.** We filter the VQA dataset for color and object number inaccuracies and correct answers with low confidence scores ( $c_o < 0.05$ ) using PROJECTAWAY. We reuse the same hyperparameters previously chosen for InstructBLIP ( $l^I = 1, l^T = 2, \alpha = 1.5$ ).

Method	InstructBLIP		LLaVA	
	mAP $\uparrow$	ROC AUC $\uparrow$	mAP $\uparrow$	ROC AUC $\uparrow$
Baseline	0.53	0.55	0.49	0.47
Ours	0.78	0.83	0.60	0.68

Table 5: **Object presence classification performance.** We use internal confidence  $c_o$  as a confidence score to classify whether the object is present in the image. We evaluate the mAP and ROC AUC of our classification method against the baseline for both the InstructBLIP and LLaVA models over a subset of 5000 COCO images.

Method	LLaVA-NeXT		Cambrian-1	
	mAP $\uparrow$	ROC AUC $\uparrow$	mAP $\uparrow$	ROC AUC $\uparrow$
Baseline	0.93	0.66	0.94	0.73
Ours	0.95	0.75	0.97	0.83

Table 6: **Object presence classification on more models.** We classify whether the object is present in the image using internal confidence for LLaVA-NeXT and Cambrian-1 over a subset of 500 COCO images.

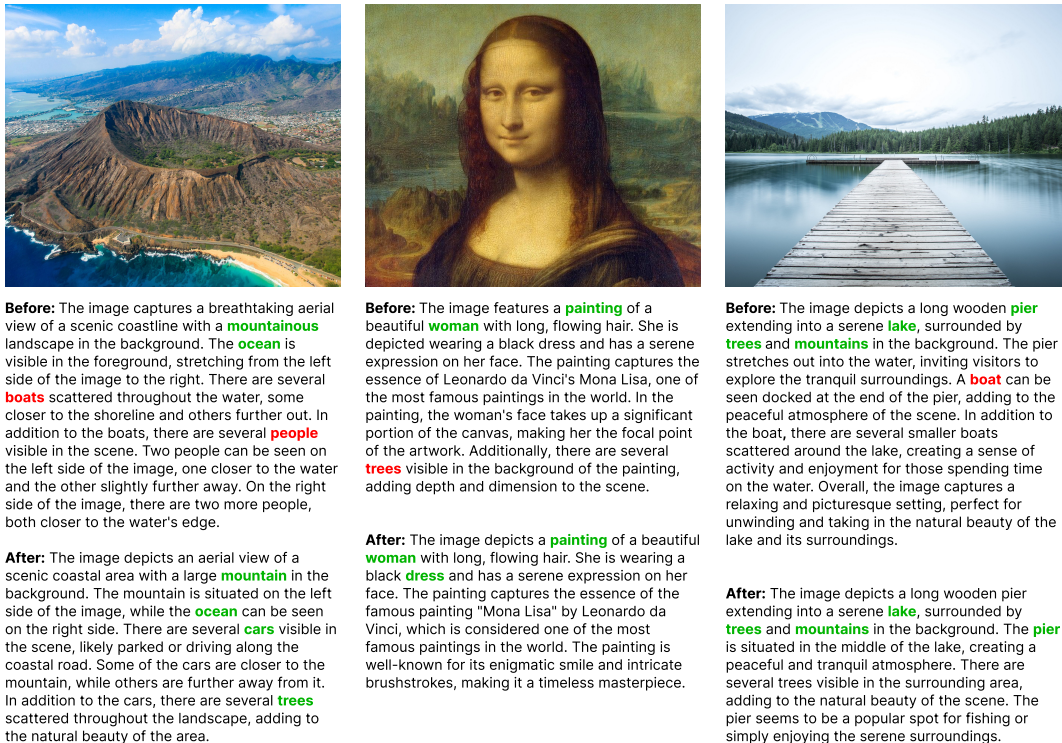


Figure 13: **Qualitative results on images from LLaVA-Bench.** We randomly select images from the benchmark and use InstructBLIP to detect and edit out hallucinations. Our hyperparameter selection is the same as in Section 4.1.1 ( $l^I = 1, l^T = 2, \alpha = 1.5$ ).

Model	Method	CHAIR <sub>i</sub> ↓	CHAIR <sub>s</sub> ↓	Recall (%) ↑
LLaVA-NeXT	Beam Search	6.8	23.8	63.12
	Ours	<b>5.52</b>	<b>17.2</b>	63.12
Cambrian-1	Beam Search	3.27	9.2	53.28
	Ours	<b>2.7</b>	<b>6.6</b>	53.28

Table 7: **Hallucination intervention performance on more models.** We mass-remove hallucinations detected by the method in Section 5.1 on two more models, LLaVA-NeXT and Cambrian-1, on the same subset of 500 COCO images as used in Table 2. We observe consistent improvement over the baseline while maintaining recall of objects present in the image.



Figure 14: LLaVA Object Presence Classification. Sample image captions from LLaVA and the internal confidence scores for objects in the caption used for classification as correctly detected objects or hallucinations.



Figure 15: InstructBLIP Object Presence Classification.



**Before:** The image depicts a **person** wearing a black shirt and gray pants, standing next to a **skateboard**. The skateboard is placed on the ground, with the person's hand resting on it. The person appears to be in the process of picking up the skateboard or preparing to ride it.

In the background, there is a **chair** and a **dining table**, suggesting that the scene might be taking place in an outdoor or semi-outdoor setting.

**After:** In the image, a **person** is standing on a sidewalk, holding a colorful skateboard in their hand. The **skateboard** features a vibrant design, making it an eye-catching sight. The person appears to be either preparing to skate or taking a break from their skateboarding session. The scene captures the essence of skateboarding culture and the enjoyment it brings to those who participate in it.



**Before:** The image shows a **person** sitting on a **bench**, holding a donut in their hand. The donut appears to be half-eaten, with a bite taken out of it. The person seems to be enjoying their snack while sitting on the bench.

In addition to the person and the donut, there is a **handbag** placed next to the person on the bench, and a **backpack** can be seen in the background.

**After:** In the image, a **person** is sitting on a **bench** and holding a pastry in their hand. The pastry appears to be a doughnut, and the person is in the process of eating it. Another doughnut can be seen on the bench, close to the person's hand. A **chair** is also visible in the scene, placed near the bench where the person is sitting.



**Before:** The image features a **man** wearing a dress shirt and tie, standing in a room. He is wearing a striped **tie**, and the shirt appears to be white. The man appears to be looking down at his tie, possibly adjusting it or checking its appearance.

In the room, there is a **couch** located towards the right side of the image, and a **chair** can be seen in the background on the left side. The man is positioned in the center of the scene, drawing attention to his attire.

**After:** The image depicts a **man** wearing a dress shirt and **tie**, standing in a room. The shirt is white, and the tie is blue. The man is wearing a belt, which is visible around his waist. The room appears to be dimly lit, creating a somewhat mysterious atmosphere. In addition to the man, there are two other people in the room, one on the left side and the other on the right side of the image. However, they are not the main focus of the scene, as the man in the dress shirt and tie is the central figure.



**Before:** The image captures a **man** in mid-air, leaping over a **bed** in a bedroom. He is wearing a white shirt and a blue **tie** and appears to be in the middle of an energetic jump. There are several other people in the room, with one person standing near the left side of the bed and two others closer to the right side. The bedroom is furnished with a **couch**, a **chair**, and a **dining table**. A **potted plant** can be seen on the right side of the room, adding a touch of greenery to the space. A **clock** is mounted on the wall, and a **cup** is placed on the dining table.

**After:** The image depicts a **man** in a white shirt and a blue **tie** jumping in the air above a bed in a bedroom. He appears to be in the process of diving onto the bed. There are several other people in the room, with some standing near the bed and others scattered around the area. The bedroom is furnished with a **dining table**, a **chair**, and a **potted plant**. There is also a **cup** placed on the dining table, and a **handbag** can be seen near one of the people in the room. Overall, the scene captures a lively and energetic atmosphere in the bedroom.



**Before:** The image captures a heartwarming scene of two **elephants**, an adult and a baby, playing together in a body of water. The **adult** elephant is partially submerged in the water, while the baby elephant is swimming nearby. They appear to be enjoying their time in the water, splashing and interacting with each other.

In addition to the two elephants, there are a few other objects in the scene. A **bench** can be seen on the left side of the image, and a **potted plant** is located near the top left corner.

**After:** The image depicts two **elephants** in a body of water, possibly a river or a lake. One of the elephants appears to be an **adult**, while the other is a baby elephant. The baby elephant is swimming in the water, while the adult elephant is standing nearby. They seem to be enjoying their time together in the water.



**Before:** The image depicts a clean and well-maintained kitchen with a white **stove** top oven. The **oven** has two burners, one on the left side and the other on the right side. Above the oven, there is a light that illuminates the cooking area. The kitchen is equipped with various utensils, including multiple **knives** and a **spoon**. The knives are placed in a knife block, while the spoon can be found on the left side of the oven. Additionally, there is a **bowl** located on the left side of the kitchen, and a **bottle** can be seen on the right side.

**After:** The image depicts a kitchen with an old-fashioned white **stove** top **oven**. The stove has four burners, with two on the left side and two on the right side. Above the stove, there is a light that illuminates the cooking area. The kitchen is well-equipped with various utensils and appliances. There are two **knives**, one on the left side of the stove and the other on the right side. Additionally, there are two **spoons**, one near the left knife and the other near the right knife. A **bottle** can be seen on the left side of the stove, and a **clock** is mounted on the wall above the oven.

Figure 16: **Qualitative results for LLaVA hallucination intervention.** Our algorithm removes hallucinations and, at times, adds correctly detected objects.



**Before:** The image depicts a young **woman** sitting on a **bench**, leaning against a wall, and talking on her **cell phone**. She is wearing a white shirt and appears to be engrossed in her conversation. In the background, there are several other people walking around, some of them carrying bags or **purses**. The scene takes place at night, with **streetlights** illuminating the area and casting shadows on the surroundings.

**After:** A young **man** is sitting on a railing, leaning against it while talking on his **cell phone**. He is wearing a **backpack** and appears to be engrossed in his conversation. There are several other people in the scene, some of whom are standing or walking around. One person is closer to the man on the railing, while others are scattered throughout the area. A **handbag** can be seen nearby, possibly belonging to one of the people in the scene.



**Before:** The image features a young **woman** sitting on a **bench** outside, eating a **hot dog** wrapped in a napkin. She appears to be enjoying her food as she takes a big bite out of the hot dog. There are several **bottles** scattered around the scene, including one close to the woman's left hand and another near her right foot. In addition to the bottles, there are two **cars** visible in the background, one on the left side and another on the right side of the image.

**After:** The image depicts a young **woman** sitting on a **bench** outside, eating a **hot dog** wrapped in a napkin. She appears to be enjoying her meal while surrounded by other **people** who are walking around the area. There are several **bottles** scattered throughout the scene, likely containing drinks or other beverages. In the background, there is a building with multiple windows visible.



**Before:** The image depicts a group of **people** riding in an old-fashioned, open-air **truck**. The truck is carrying a large number of people, with some sitting on the bed of the truck and others standing around it. There are several **umbrellas** in the scene, one of which is held by a person in the back of the truck, providing shade for the passengers. In addition to the umbrella, there are several **handbags** scattered throughout the scene, likely belonging to the passengers. The truck appears to be making its way through a wooded area, surrounded by trees and foliage.

**After:** The image features a group of **people** riding in an old-fashioned, open-air vehicle, likely an old tractor or **truck**, on a dirt road surrounded by trees. They are enjoying a leisurely ride through the countryside, with one person holding a purple **umbrella** to protect themselves from the sun. There are several people in the vehicle, with some seated in the front and others in the back. The scene captures the essence of a relaxed and enjoyable day out in the countryside.



**Before:** The image depicts a group of four young **men** playing a game of **frisbee** on a grassy field. They are all wearing orange shirts, and one of them is jumping up to catch the frisbee as it flies through the air. There are several **benches** scattered around the field, providing seating options for the players and spectators. In addition to the benches, there are two **backpacks** visible in the scene, likely belonging to the players or spectators. Overall, the scene captures a lively and energetic game of frisbee among friends.

**After:** There is a group of young **men** playing a game of **frisbee** on a soccer field. They are all wearing matching shirts, and one of them is jumping up to catch the frisbee as it flies through the air. The other players are also actively participating in the game, trying to catch the frisbee or block their opponents' attempts to score. There are several **benches** scattered around the field, providing seating for those watching the game or taking a break from the action.



**Before:** The image depicts a city street with a red and white public transit **bus** parked on the side of the road. The bus is surrounded by other vehicles, including **cars**, **trucks**, and a **motorcycle**. There are several **people** visible in the scene, some standing near the bus and others walking along the sidewalk. A **bicycle** is also present in the scene, likely belonging to one of the pedestrians. Overall, the scene showcases a busy urban environment with various modes of transportation in use.

**After:** A red and white city **bus** is parked on the side of a street, waiting for passengers to board. There are several **people** in the vicinity of the bus, including one person standing near the front of the bus, another person walking towards the bus, and a third person further away from the bus. A **bicycle** is also visible in the scene, likely belonging to one of the pedestrians. In the background, there is a **car** parked on the other side of the street.



**Before:** The image depicts a cozy living room filled with various furniture and decorations. There is a black **couch** placed in the center of the room, surrounded by several **potted plants**. On the left side of the room, there is a coffee table with two **cups** placed on it. A **television** can be seen on the right side of the room, positioned close to the wall. In addition to the couch and coffee table, there are several potted plants scattered throughout the room, adding a touch of greenery to the space. Two **bottles** are also visible, one on the left side of the room and the other on the right side, near the coffee table. Overall, the living room has a warm and inviting atmosphere, perfect for relaxing and spending time with friends or family.

**After:** The image depicts a well-appointed living room with a **couch**, coffee table, and a **dining table**. There are several **potted plants** scattered throughout the room, adding a touch of greenery to the space. A bookshelf is visible on the left side of the room, showcasing various **books** and decorative items. In the center of the room, there is a coffee table surrounded by **chairs**, providing a comfortable seating area for guests. The room has a cozy and inviting atmosphere, perfect for relaxation and social gatherings.

Figure 17: Qualitative results for InstructBLIP hallucination intervention.

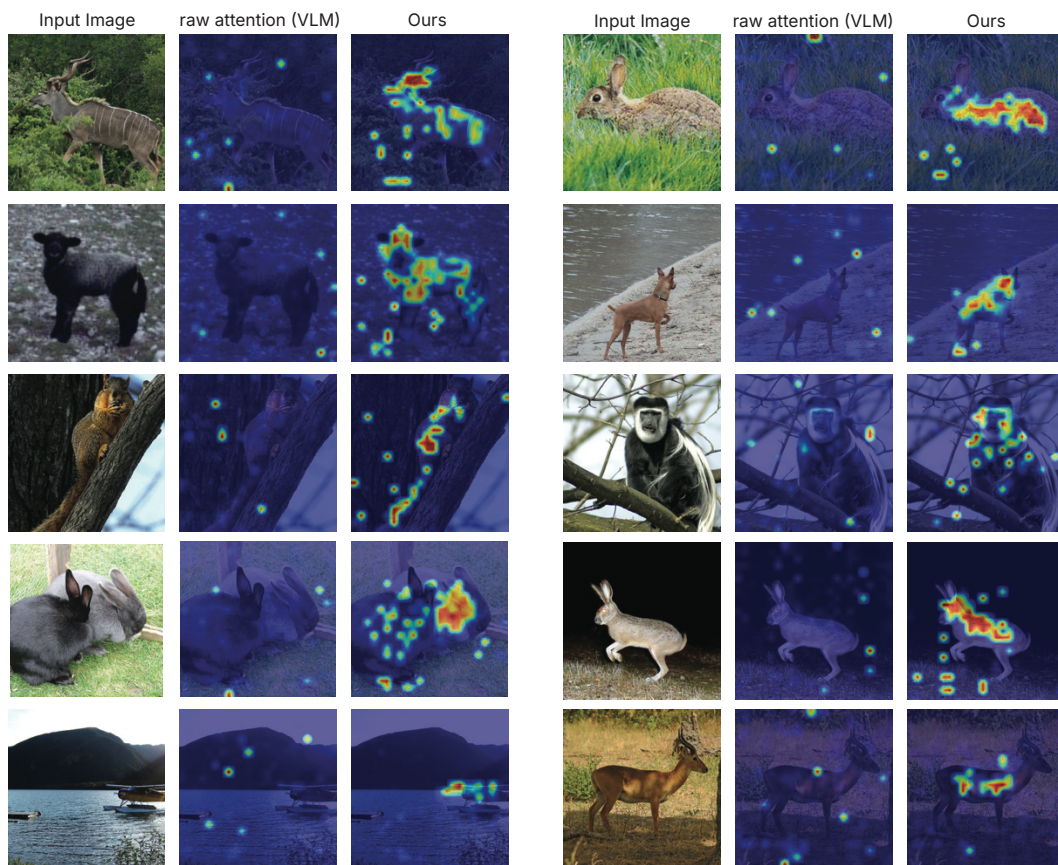


Figure 18: Object Localization Samples.

Class	T3%	T5%	T10%	Patches	Class	T3%	T5%	T10%	Patches
airplane	51.0	61.8	72.5	102	kite	66.7	77.8	88.9	9
apple	70.2	76.6	80.9	47	knife	24.0	26.0	34.0	50
backpack	44.8	48.5	58.5	614	laptop	34.1	38.3	46.1	334
banana	77.2	79.2	83.2	101	microwave	23.8	37.2	55.2	223
baseball bat	0.0	33.3	33.3	3	motorcycle	64.7	70.6	78.3	984
baseball glove	65.4	69.2	73.1	26	mouse	50.0	50.0	66.7	6
bear	37.6	41.4	47.6	739	orange	44.2	50.0	57.7	52
bed	44.0	47.8	52.0	2373	oven	38.9	54.4	78.9	507
bench	61.3	63.9	66.6	524	parking meter	20.9	24.8	29.6	230
bicycle	27.2	32.3	58.3	235	person	0.5	1.1	12.6	11528
bird	75.5	79.4	80.6	155	pizza	41.8	52.1	69.4	3146
boat	26.2	29.7	38.8	516	potted plant	43.8	52.1	63.0	192
book	28.1	39.0	44.8	210	refrigerator	23.7	31.4	50.0	156
bottle	46.2	53.4	62.0	208	remote	14.3	17.3	17.3	98
bowl	22.1	25.0	31.9	1364	sandwich	40.2	44.4	54.3	468
broccoli	75.9	77.2	79.7	79	scissors	71.9	71.9	71.9	32
bus	49.8	54.1	61.3	1786	sheep	49.5	52.6	56.6	489
cake	43.2	51.4	83.5	1182	sink	57.0	60.3	65.1	272
car	29.4	37.7	52.7	714	skateboard	48.1	50.6	57.7	239
carrot	50.0	50.0	75.0	4	skis	27.6	34.2	44.7	76
cat	57.7	61.5	66.5	2239	snowboard	37.5	41.7	47.9	48
cell phone	73.4	76.6	82.8	64	spoon	35.5	43.5	53.2	62
chair	31.6	33.1	37.6	516	sports ball	4.4	8.9	20.0	45
clock	67.6	70.6	75.9	299	stop sign	85.7	88.6	89.9	237
couch	33.4	38.9	63.2	2435	suitcase	38.1	40.7	44.7	472
cow	51.9	58.6	67.0	324	surfboard	48.6	57.5	69.9	146
cup	9.4	14.9	30.4	181	teddy bear	38.5	43.1	47.7	239
dining table	25.4	47.6	74.9	7403	tennis racket	88.9	88.9	88.9	9
dog	45.9	51.3	59.7	1057	tie	46.2	49.7	52.8	197
donut	34.8	40.0	45.2	115	toilet	92.0	97.3	99.6	1131
elephant	47.0	57.4	64.9	902	toothbrush	78.9	78.9	100.0	19
fire hydrant	43.4	47.0	50.1	419	traffic light	45.5	45.5	45.5	11
fork	41.4	45.7	54.3	70	train	40.7	45.0	52.1	3008
frisbee	50.0	60.6	71.2	66	truck	34.5	40.1	54.6	930
giraffe	32.0	39.8	62.8	810	tv	27.2	32.6	37.6	298
handbag	42.2	53.0	57.8	83	umbrella	39.5	40.5	42.8	526
horse	63.7	65.8	68.8	240	vase	29.9	32.6	45.1	264
hot dog	56.9	62.7	69.3	394	wine glass	61.9	67.0	74.3	218
keyboard	43.1	47.7	49.2	65	zebra	33.0	35.9	44.5	373
<b>Overall</b>	<b>32.7</b>	<b>39.3</b>	<b>52.2</b>	<b>55988</b>					

Table 8: **Per-class patch classification accuracy.** For each COCO class, we show the percentage of patches containing that object that top-k logit lens predictions can correctly identify.